Charge Oscillation Controlled Molecular Excitation

Tim Bayer,[1] Hendrike Braun,[1] Cristian Sarpe,[1] Robert Siemering,[2] Philipp von den Hoff,[2] Regina de Vivie-Riedle,[2] Thomas Baumert,[1] and Matthias Wollenhaupt[1,*]

[1]*Institut für Physik und CINSaT, Universität Kassel, Heinrich-Plett-Strasse 40, 34132 Kassel, Germany*

[2]*Department Chemie, Ludwig-Maximilians-Universität München, Butenandt-Strasse 11, 81377 München, Germany*

(Received 12 December 2012; revised manuscript received 18 February 2013; published 22 March 2013)

The direct manipulation of charge oscillations has emerged as a new perspective in chemical reaction control. Here, we demonstrate, in a joint experimental and theoretical study, that the electron dynamics of a molecule is efficiently steered by controlling the interplay of a driving femtosecond laser pulse with the photoinduced charge oscillation. These oscillations have a typical Bohr period of around 1 fs for valence electrons; therefore, control has to be exerted on a shorter time scale. Specifically, we show how precision pulse shaping is used to manipulate the coupled electron and nuclear dynamics in order to address different bound electronic target states in a molecule. We present a strong-field coherent control mechanism which is understood in terms of a simple classical picture and at the same time verified by solving the time-dependent Schrödinger equation. This mechanism is universally applicable and opens a wide spectrum of applications in the reaction control of complex systems.

DOI: 10.1103/PhysRevLett.110.123003 PACS numbers: 32.80.Qk, 32.80.Rm, 42.50.Md

The ability to control the course and the outcome of chemical reactions using coherent light [1] has become realistic with the experimental accessibility of femtosecond laser pulses acting on the natural time scale of nuclear motion driving chemical reactions [2]. With the advent of sophisticated pulse shaping techniques [3,4], efficient control on these very processes became available [5]. New frontiers opened with the realization of attosecond pulses in the laboratory. The emerging field of attosecond science [6–9] provided the possibility to directly observe even faster electron dynamics. Because of the high photon energies, the excitation of outer shell electrons by attosecond laser fields suffers from low cross sections and is likely to cause direct ionization, hampering the implementation of valence bond chemistry control schemes. On the other hand, electronic transitions of outer shell electrons driven by pico- to femtosecond laser pulses benefit from large transition moments. This is a prerequisite for efficient population transfer and thus to achieve efficient product yields in reaction control. In addition, nonperturbative strong laser fields alter the potential energy surface (PES) via dynamic Stark shifts, exploring new routes to different target states inaccessible in the weak-field regime. Experimental demonstrations of nonresonant Stark control acting on the time scale of the intensity envelope of an ultrashort laser pulse [10] comprise the observation of non-Franck-Condon transitions in bound wave packet motion [11], population control in atoms by shaped laser pulses [12], control of bound vibrational levels [13], and control of the branching ratio in a dissociation reaction [14]. The resonant Stark effect, acting on the time scale of the electron dynamics, provides more efficient manipulation of the energy landscape and in particular enables Stark shifting of molecular states to higher as well as lower energies [15–18].

In this Letter, we present a resonant coherent control scheme based on shaped intense femtosecond laser pulses where the initial part of the laser pulse creates an oscillating charge distribution with maximum amplitude in a molecule. After evolution on coherently coupled PES, a later part of the laser pulse is timed with extreme precision [19] to adjust the phase of the field to the oscillating dipole. The scenario allows us to steer the coupled electron and nuclear motion of the molecule to selectively populate different target channels, each of which entails different subsequent nuclear dynamics. Theoretical studies on the selective population of a single target channel employing pulse sequences used the potassium dimer (K_2) as the molecular prototype system [20–22]. Here, we report on the first experimental implementation of this control mechanism on molecules. For a proof of principle study, we also use the K_2 molecule because this system can be studied experimentally and theoretically on an equally accurate level. Quantum dynamical studies confirmed that the selectivity of the switching process is caused by the induced electronic coherence. Figure 1(a) shows the scheme for the selective excitation of K_2 with near 800 nm laser pulses. The molecular system consists of the $X^1\Sigma_g^+$ ground state, a resonant intermediate state ($A^1\Sigma_u^+$), and a set of final target states for selective population. The insets display calculated three-dimensional electronic density distributions for the relevant molecular states. In addition, the electronic densities for the superposition states of the $X^1\Sigma_g^+$ and $A^1\Sigma_u^+$ and their resulting dipole moments are shown. For computational details, see the Supplemental Material [23]. Weak-field interaction (red arrows) excites the molecule from the vibronic ground state $X^1\Sigma_g^+$ to the $2^1\Pi_g$ state via the resonant state $A^1\Sigma_u^+$. Strong-field resonant interaction initially results in a charge oscillation in

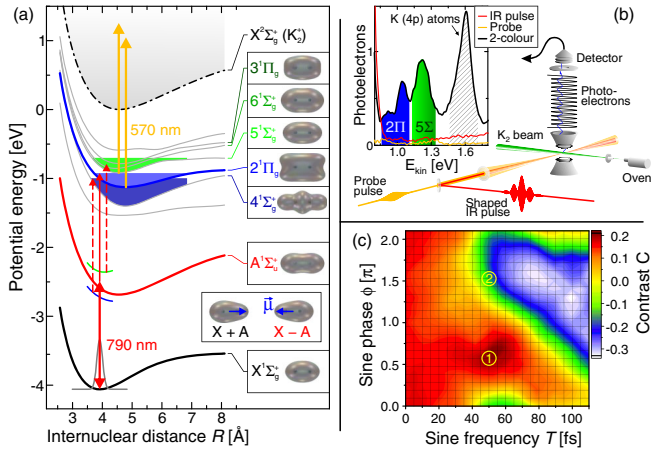

FIG. 1 (color online). (a) Excitation and detection scheme, (b) experimental setup and measured photoelectron signals, and (c) measured contrast landscape. For details, see the text.

the X-A subsystem, visualized by the distinct electronic superpositions of maximum coherence. The PESs are modified, and the corresponding dressed states (indicated by short blue and green line segments above and below the $A^1\Sigma_u^+$ PES around $R = 3.9$ Å) give access to lower (blue-shaded area between the $4^1\Sigma_g^+$ and the $2^1\Pi_g$ PES) and higher-lying (green-shaded area between the $5^1\Sigma_g^+$ and the $3^1\Pi_g$ PES) electronic target states. In the experiment, a probe pulse (yellow arrows) photoionizes the excited molecule and maps the target state populations into the photoelectron spectrum.

This strong-field control scenario can be realized by a double pulse sequence consisting of a moderately strong preparation pulse followed by a more intense main pulse [17,20,24]. In this scenario, both pulses are resonant with the X-A transition. This pulse sequence permits a transparent analysis of the physical mechanism. The preparation pulse gives rise to an *electronic* coherence in the X-A subsystem, launching an electronic wave packet. The time evolution of the electronic wave packet is reflected in the oscillating dipole moment $\vec{\mu}(t)$. The dipole oscillates with a molecular Bohr period proportional to the energy difference in the X-A subsystem of about 2.8 fs. Analogous to a classical oscillator driven on resonance, the induced dipole initially follows the driving field with a phase shift of $-\pi/2$. The subsequent intense main pulse interacts with the dipole, giving rise to an interaction energy $\varepsilon(t) = -\vec{\mu}(t) \cdot \vec{E}(t)$ that is analogous to a classical dipole in an electric field. The interaction energy is controlled precisely by the phase relation in the scalar product. A main pulse which is timed to oscillate out of phase with the previously induced dipole *maximizes* $\varepsilon(t)$. Higher-lying electronic target states become energetically accessible and are excited selectively. Shifting the main pulse in time by half an optical cycle causes in-phase oscillations of the laser and the dipole. This leads to *minimization* of $\varepsilon(t)$, i.e., to selective excitation of lower-lying electronic target states. In a quantum mechanical framework, maximization (minimization) of the interaction energy corresponds to selective population of a dressed state (SPODS) [25]. Here, this means selective population of the upper (lower) molecular dressed state of the resonant X-A subsystem. The dressed state energy splitting is proportional to the amplitude of the electric field.

Following these arguments, high precision phase control to suitably adapt the laser field to the induced dipole dynamics ($\vec{E}$ and $\vec{\mu}$ antiparallel or parallel) in combination with amplitude control to adapt the interaction energy to the separation of the target states, i.e., several 100 meV [17], are the ingredients for selective excitation on the ultrafast time scale.

In practice, the straightforward implementation using a double pulse sequence does not always lead to the optimal controllability of molecular systems [20,21]. In general, the light-induced electric dipole is subject to additional phase dynamics due to vibrational wave packet propagation on the PESs during the interaction with the laser pulse; i.e., the electronic resonance becomes time dependent, introducing dynamic detuning. This coupling between electron and nuclear motion influences the amplitude and phase of the coherent charge oscillation. Thus, the interplay between the driving laser field, which simultaneously induces and controls the dipole dynamics, and the driven molecule is more complex. To allow for this complexity, we used more versatile pulse shapes in terms of both temporal amplitude and phase. To this end, we applied a sinusoidal phase modulation $\varphi(\omega) = A \sin[T(\omega - \omega_0) + \phi]$ to our laser spectrum. This spectral phase modulation yields a multipulse sequence [17,26–28]. The features of the sequence are adjusted by the phase parameters A, T, and ϕ. The sine amplitude A determines the amplitudes of the subpulses; their temporal separation is given by the sine frequency T. The sine phase ϕ controls the relative temporal phases between adjacent subpulses and exerts phase control on the electric dipole dynamics.

A schematic of the experimental setup is displayed in Fig. 1(b); for further details, see Ref. [23]. An amplified Ti:sapphire laser system provides pulses of 25 fs FWHM at a central wavelength of about 790 nm. Because of the blue detuning of the laser spectrum with respect to the X-A resonance (846 nm at $R_0 = 3.9$ Å), the system is biased toward excitation of the $2^1\Pi_g$ state. Under these conditions, we observe switching between the states $2^1\Pi_g$ and $5^1\Sigma_g^+$ rather than between the states $4^1\Sigma_g^+$ and $5^1\Sigma_g^+$, as discussed in the theory [20]. The amplified IR pulses are spectrally phase modulated according to $\varphi(\omega)$ using our home-built Fourier transform pulse shaper based on a liquid crystal spatial light modulator. The shaped IR pulses are focused into a potassium supersonic molecular beam. The laser and molecular beams intersect between the pole plates of a magnetic bottle time-of-flight photoelectron spectrometer. In the experiments on K_2, the final

population in the neutral electronic target channels is measured by photoionization and detection of photoelectrons. Ionization is triggered by a 570 nm probe pulse [yellow photon arrows in Fig. 1(a)] from an optical parametric amplifier, which follows the shaped IR pulse collinearly into the interaction region, allowing for nearly background-free detection of photoelectrons from the molecular target states $2^1\Pi_g$ and $5^1\Sigma_g^+$, as seen in the measured photoelectron spectrum in Fig. 1(b) (for more details, see Ref. [23]). The photoelectrons from the $2^1\Pi_g$ state are a measure for the final population in the lower electronic target channel. Photoelectrons from the target states $5^1\Sigma_g^+$, $6^1\Sigma_g^+$, and $3^1\Pi_g$ are a measure for the final population in the upper electronic target channel. For simplicity, we will refer to the entire upper target channel contribution as the $5^1\Sigma_g^+$ signal. For the following discussions, we introduce the contrast $C = (S_{5\Sigma} - S_{2\Pi})/(S_{5\Sigma} + S_{2\Pi})$ between the integrated signal yields $S_{2\Pi}$ [blue-shaded area in the inset to Fig. 1(b)] and $S_{5\Sigma}$ (green-shaded area), as a scalar measure for the selectivity achieved in the population of a specific electronic target channel.

First, we investigated the intensity dependence of the population transfer to the electronic target channels by the bandwidth-limited IR pulse. This procedure provides an unambiguous check on the strong-field nature of the excitation process and rules out perturbative scenarios such as spectral interference. Our findings (see Supplemental Fig. 2) confirm that, in the weak-field limit, i.e., for laser intensities smaller than 1×10^{11} W/cm^2, only the $2^1\Pi_g$ state is accessible. Efficient population of higher-lying target states is only achieved above a threshold intensity of about 5×10^{11} W/cm^2. This observation proves the nonperturbative character of the scenario. Subsequently, we studied strong-field *phase* control on the K_2 molecule. To this end, we chose a fixed IR pulse intensity of 8.5×10^{11} W/cm^2, at which the upper target channel was populated most efficiently and almost selectively by the bandwidth-limited pulse. The sine amplitude was set to $A = 0.8$ rad, which was found to provide a high degree of control on both the upper and the lower target channel yields. The experimental result of a systematic variation of the phase parameters T and ϕ is illustrated in Fig. 1(c) in terms of a two-dimensional contrast landscape.

A pronounced maximum is found around $T = 50$ fs and $\phi = 1.8$ rad with $C = 0.21$ [see Fig. 1(c), label 1], the high sine frequency of $T = 50$ fs hinting to vibrational wave packet dynamics. The corresponding photoelectron spectrum is shown in Fig. 2(a). The photoelectron yield

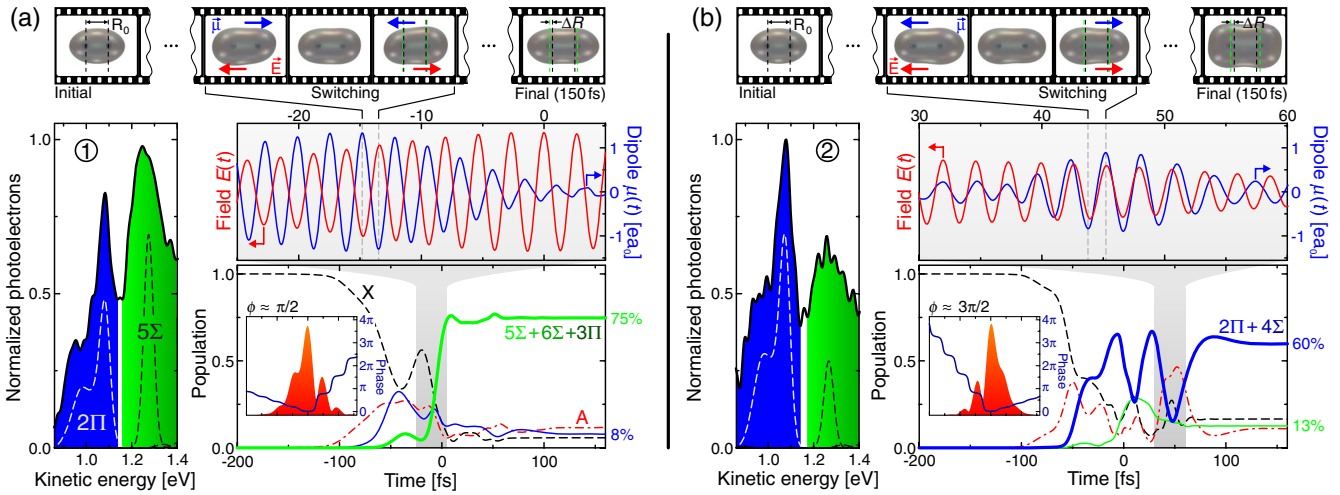

FIG. 2 (color online). Experimental and theoretical results for the excitation of K_2 molecules with two different pulse shapes, leading to population of (a) the upper target state $5^1\Sigma_g^+$ and (b) the lower target state $2^1\Pi_g$. On both sides, the left frame shows the measured photoelectron spectra (black line, signal contributions colored accordingly) compared to simulations, taking focal intensity and molecular orientation averaging into account (dashed lines). To the right of these spectra, the neutral electronic population dynamics are shown, along with the driving shaped IR pulses, decomposed into their temporal amplitude (red background) and phase (blue line), as insets. The black dashed line represents the ground state $X^1\Sigma_g^+$, the red dash-dotted line the intermediate state $A^1\Sigma_u^+$. For clarity, the blue and green curves represent the accumulated populations of the lower (i.e., the $2^1\Pi_g$ and the $4^1\Sigma_g^+$ states) and upper (i.e., the $5^1\Sigma_g^+$, $6^1\Sigma_g^+$, and $3^1\Pi_g$ states) electronic target channels. The phase relation of the electric field $E(t)$ (red line) and the induced electric dipole moment $\mu(t)$ of the X-A subsystem (blue line) is illustrated in the upper right frame. It depicts the interplay of dipole and field during the switching time window (gray-shaded background) where the population transfer to the electronic target channels takes place. The amplitude and phase modulation of the electronic dipole with respect to the constant electric field directly reflects the coupling between the nuclear and electronic motion. Out-of-phase (in-phase) oscillation of μ and E, as on the left-hand (right-hand) side, maximizes (minimizes) the interaction energy and results in efficient population of the upper (lower) electronic target channel. The movies on top show snapshots of the driven charge oscillation for decisive moments during the laser-molecule interactions.

of the upper target channel exceeds the one generated by the bandwidth-limited IR pulse that is also included in the landscape in Fig. 1(c) for $T = 0$ fs with a contrast of $C = 0.12$, proving efficient population of the upper target channel. Simultaneously, the low yield of photoelectrons from the lower target channel indicates the selectivity achieved by the shaped IR pulse. From the basic control scheme derived on atoms, we expect switching from the upper to the lower target channel by a change of the sine phase by $\Delta\phi = \pi$ [17] as the signature of SPODS. Indeed, we find efficient population of the lower target channel at a phase shift of about π at a fixed subpulse separation of $T = 50$ fs with $C = -0.2$; see Fig. 1(c), label 2, and Fig. 2(b) for the measured photoelectron spectrum. Here, the high photoelectron signal from the lower target channel together with the low signal from the upper target channel indicate selective and efficient population of the lower electronic target channel. Generally, the regions of selective excitation are not as sharply defined as in atoms due to molecular orientation averaging. To extract a realistic picture of the underlying control mechanism for the distinct pulse shapes shown in Figs. 2(a) and 2(b), we carried out quantum dynamics simulations. The calculations included the coupled nuclear and electronic wave packet propagation induced by the intense shaped IR pulses. This approach allows us to visualize and follow the prepared oscillating dipole $\mu(t)$. A detailed description of the numerical techniques applied in the calculations is given in Refs. [20,23,29]. We model the K_2 molecule by seven electronic states, cf. Fig. 1(a), and approximate the experimental parameters by a Gaussian-shaped input pulse centered at 800 nm with a FWHM duration of 30 fs. The input pulse is sinusoidally phase modulated in the frequency domain according to $\varphi(\omega)$. To elucidate the underlying control mechanism, we assume the shaped IR pulses to be polarized at 45° with respect to the internuclear axis of the diatomic molecule for the simulation of the population dynamics. Thus, parallel ($\Sigma \leftarrow \Sigma$) and perpendicular ($\Pi \leftarrow \Sigma$) transitions are driven by the same intensity. For the actual comparison between measured and simulated photoelectrons, however, we consider both focal intensity averaging and molecular orientation averaging in order to model the experimental conditions. The measured photoelectron spectra and the results of the simulations are presented in Fig. 2. For a detailed description of the displayed quantities, we refer to the figure caption. The measured two-color photoelectron spectrum associated with the pulse shape (a) is characterized by a pronounced $5^1\Sigma_g^+$ signal that clearly exceeds the contribution from the $2^1\Pi_g$ state. Initially, between -100 and -50 fs, the laser field guides the ground state $X^1\Sigma_g^+$ and the resonant intermediate state $A^1\Sigma_u^+$ into a coherent electronic superposition, launching the oscillating electric dipole. In the switching time window, the dipole oscillates with maximum amplitude exactly out of phase with the electric field of the main pulse. The intense central subpulse opens the upper target channel energetically and, due to the maximization of the interaction energy $\varepsilon(t)$, transfers the population efficiently to the high-lying set of target states. The lower electronic target channel remains nearly unpopulated. During the time between the buildup of the electronic coherence and the switching time, the internuclear distance increases by 8% due to the vibrational dynamics, resulting in a change of the Bohr frequency of 100 meV. This coupling between the nuclear and electronic motions is directly reflected in the amplitude and phase modulations of the electric dipole in relation to the driving laser field, as stated in the introduction, and would not be seen in the case of a resonantly driven atom. The good agreement of the measured and simulated photoelectron spectra confirms the high degree of control achieved in the experiment. For the width of the simulated signals, a spectrometer resolution of 50 meV (at 1.2 eV) was taken into account. Additional broadening due to the width of the optical parametric amplifier probe spectrum (70 meV) was not considered. The simulation results for the pulse shape (b) are presented on the right-hand side of Fig. 2. In the measured and calculated photoelectron spectra, a considerable enhancement of the $2^1\Pi_g$ at the expense of the $5^1\Sigma_g^+$ signal is observed. Inspection of the population dynamics reveals again a buildup of the X-A coherence between -100 and -50 fs. After this time period, a more complicated population dynamics is observed. Rabi cycling in the lower electronic target channel occurs due to the fact that (i) the transition dipole moment between states $2^1\Pi_g$ and $A^1\Sigma_u^+$ is larger than the corresponding coupling between states $5^1\Sigma_g^+$ and $A^1\Sigma_u^+$ [20] and (ii) the lower target channel is always accessible energetically. However, after the completion of the second Rabi cycle, around 45 fs, the dipole increases once more and shifts in phase with the shaped laser pulse during the switching time window. Thus, the interaction energy $\varepsilon(t)$ is minimized and the lower target states are populated efficiently, while the upper electronic target channel remains almost unpopulated. Owing to the longer time until the switching occurs, the internuclear separation has by then increased by 11% and the frequency of the oscillating dipole is changed by 130 meV.

The electron movies in the upper panels of Fig. 2 visualize the spatial aspects of the induced electronic and nuclear motion together with the associated dipole moment $\vec{\mu}(t)$ (blue arrows) and the applied electric field $\vec{E}(t)$ (red arrows). Starting from the ground state configuration, the movies proceed via the transient electron dynamics during the switching time window and end with the molecule in its final electronic configuration. The vertical black and green dashed lines indicate the nuclear dynamics during the interaction. On the left-hand side, the induced dipole and the electric field oscillate strictly out of phase, steering the molecule into a peanut-shaped electron configuration dominated by the $5^1\Sigma_g^+$ electron density distribution

[cf. Fig. 1(a)]. On the right-hand side, $\vec{\mu}(t)$ and $\vec{E}(t)$ oscillate strictly in phase. As a result, the molecule is guided into a cushionlike electronic configuration, clearly reflecting the $2^1\Pi_g$ electron density distribution.

We demonstrated efficient ultrafast switching between bound electronic target states in a molecule by intense femtosecond laser pulses shaped with attosecond precision. It was shown how accurate phase control of photoinduced electron dynamics combined with specific manipulation of the potential energy landscape using resonant strong laser fields allows us to steer the molecular system efficiently into a preselected electronic target channel. The key to strong-field control of coupled electron-nuclear dynamics is tailoring the phase of the driving laser field to the charge oscillation of the induced electron wave packet. We note that signatures of this control scenario have also been observed in the controlled fragmentation of isopropyl alcohol [5]. Promising applications of the presented scenario therefore range from ultrafast coherent control of valence bond chemistry in complex systems to efficient ultrafast switching in quantum information processing [30].

The Kassel group gratefully acknowledges financial support by the Deutsche Forschungsgemeinschaft (DFG) and the Otto Braun Fonds. This work was furthermore supported by the European Commission Project FASTQUAST. The Munich group gratefully acknowledges support by the DFG via the Cluster of Excellence: Munich Centre of Advanced Photonics, the SFB749, and the Normalverfahren.

*wollenhaupt@physik.uni-kassel.de

[1] M. Shapiro and P. Brumer, *Quantum Control of Molecular Processes* (Wiley-VCH, Berlin, 2011) and references therein.
[2] A. Zewail, J. Phys. Chem. A **104**, 5660 (2000).
[3] A. M. Weiner, Opt. Commun. **284**, 3669 (2011).
[4] T. Brixner, G. Krampert, T. Pfeifer, R. Selle, G. Gerber, M. Wollenhaupt, O. Graefe, C. Horn, D. Liese, and T. Baumert, Phys. Rev. Lett. **92**, 208301 (2004).
[5] M. Wollenhaupt and T. Baumert, Faraday Discuss. **153**, 9 (2011) and references therein.
[6] P. B. Corkum and F. Krausz, Nat. Phys. **3**, 381 (2007).
[7] M. F. Kling and M. J. J. Vrakking, Annu. Rev. Phys. Chem. **59**, 463 (2008).
[8] F. Krausz and M. Ivanov, Rev. Mod. Phys. **81**, 163 (2009).
[9] F. Remacle and R. D. Levine, Proc. Natl. Acad. Sci. U.S.A. **103**, 6793 (2006).
[10] P. J. Bustard, G. Wu, R. Lausten, D. Townsend, I. A. Walmsley, A. Stolow, and B. J. Sussman, Faraday Discuss. **153**, 321 (2011).
[11] T. Frohnmeyer, M. Hofmann, M. Strehle, and T. Baumert, Chem. Phys. Lett. **312**, 447 (1999).
[12] C. Trallero-Herrero, J. L. Cohen, and T. Weinacht, Phys. Rev. Lett. **96**, 063603 (2006).
[13] H. Goto, H. Katsuki, H. Ibrahim, H. Chiba, and K. Ohmori, Nat. Phys. **7**, 383 (2011).
[14] B. Sussman, D. Townsend, M. Ivanov, and A. Stolow, Science **314**, 278 (2006).
[15] S. H. Autler and C. H. Townes, Phys. Rev. **100**, 703 (1955).
[16] C. Meier and V. Engel, Phys. Rev. Lett. **73**, 3207 (1994).
[17] M. Wollenhaupt, D. Liese, A. Präkelt, C. Sarpe-Tudoran, and T. Baumert, Chem. Phys. Lett. **419**, 184 (2006).
[18] A. Palacios, H. Bachau, and F. Martín, Phys. Rev. A **74**, 031402 (2006).
[19] J. Köhler, M. Wollenhaupt, T. Bayer, C. Sarpe, and T. Baumert, Opt. Express **19**, 11 638 (2011).
[20] M. Wollenhaupt and T. Baumert, J. Photochem. Photobiol., A **180**, 248 (2006).
[21] P. von den Hoff, M. Kowalewski, and R. de Vivie-Riedle, Faraday Discuss. **153**, 159 (2011).
[22] J. Petersen and R. Mitrić, Phys. Chem. Chem. Phys. **14**, 8299 (2012).
[23] See Supplemental Material at http://link.aps.org/supplemental/10.1103/PhysRevLett.110.123003 for further details.
[24] T. Bayer, M. Wollenhaupt, C. Sarpe-Tudoran, and T. Baumert, Phys. Rev. Lett. **102**, 023004 (2009).
[25] M. Wollenhaupt, A. Präkelt, C. Sarpe-Tudoran, D. Liese, and T. Baumert, J. Opt. B **7**, S270 (2005).
[26] D. Meshulach and Y. Silberberg, Nature (London) **396**, 239 (1998).
[27] J. Herek, R. Wohlleben, R. Cogdell, D. Zeidler, and M. Motzkus, Nature (London) **417**, 533 (2002).
[28] M. Wollenhaupt, A. Präkelt, C. Sarpe-Tudoran, D. Liese, T. Bayer, and T. Baumert, Phys. Rev. A **73**, 063409 (2006).
[29] P. von den Hoff, I. Znakovskaya, M. F. Kling, and R. de Vivie-Riedle, Chem. Phys. **366**, 139 (2009).
[30] R. de Vivie-Riedle and U. Troppmann, Chem. Rev. **107**, 5082 (2007).